RESEARCH ARTICLE | DECEMBER 04 2024

Indium-flush technique for C-band InAs/InP quantum dots

Jiajing Yuan ; Calum Dear ; Hui Jia ; Jae-Seong Park ; Yaonan Hou ; Khalil El Hajraoui ; Haotian Zeng ; Huiwen Deng ; Junjie Yang ; Mingchu Tang ; Siming Chen ; Quentin M. Ramasse ; Qiang Li ; Alwyn Seeds ; Huiyun Liu

APL Mater. 12, 121109 (2024)
https://doi.org/10.1063/5.0239360

Indium-flush technique for C-band InAs/InP quantum dots

Cite as: APL Mater. 12, 121109 (2024); doi: 10.1063/5.0239360
Submitted: 23 September 2024 • Accepted: 18 November 2024 •
Published Online: 4 December 2024

Jiajing Yuan,[1] Calum Dear,[1] Hui Jia,[1,a)] Jae-Seong Park,[1,a)] Yaonan Hou,[2] Khalil El Hajraoui,[3,4] Haotian Zeng,[1] Huiwen Deng,[1] Junjie Yang,[1] Mingchu Tang,[1] Siming Chen,[1] Quentin M. Ramasse,[3,5] Qiang Li,[6] Alwyn Seeds,[1] and Huiyun Liu[1]

AFFILIATIONS

[1] Department of Electronic and Electrical Engineering, University College London, London WC1E 7JE, United Kingdom
[2] Department of Electronic and Electrical Engineering, Bay Campus, Swansea University, Swansea SA1 8EN, United Kingdom
[3] SuperSTEM, SciTech Daresbury Science and Innovation Campus, Block J, Keckwick Lane, Daresbury WA4 4AD, United Kingdom
[4] York NanoCentre & Department of Physics, University of York, York YO10 5DD, United Kingdom
[5] School of Chemical and Process Engineering and School of Physics and Astronomy, University of Leeds, Leeds LS2 9JT, United Kingdom
[6] School of Physics and Astronomy, Cardiff University, Cardiff CF24 3AA, United Kingdom

[a)] **Authors to whom correspondence should be addressed:** hui.jia@ucl.ac.uk and jae-seong.park@ucl.ac.uk

ABSTRACT

High-quality InAs/InP quantum dots (QDs) emitting at 1550 nm are indispensable to realize high-performance telecom C-band lasers. In general, a longer emission (>1550 nm) with a broad spectral character has been obtained with InAs/InP QDs. Here, we proposed the use of the indium-flush (IF) method to shorten the emission and improve the optical properties of InAs/InP QDs. By exploiting IF, the full-width at half-maximum of the room-temperature QD photoluminescence spectra is narrowed from 89.2 to 47.9 meV, with a blue shift of 300 nm (from 1824 to 1522 nm). The scanning transmission electron microscopy and electron energy loss spectroscopy results reveal the atomic-level mechanism of the IF method, which uniformly modify the height of InAs/InP QDs in a controlled manner and form distinct Al-rich and In-rich regions. Finally, InAs/InP (001) QD lasers with the IF method have been demonstrated with a low threshold current density per QD layer of 106 A/cm^2. We demonstrated both in terms of mechanism model and device performance that the IF method could serve as a robust strategy for the growth of high-performance C-band InAs/InP QD lasers via molecular beam epitaxy.

I. INTRODUCTION

Self-assembled InAs quantum dots (QDs) grown by the Stranski–Krastanov (S–K) mode have attracted considerable attention in various optoelectronic applications, including photodetectors, lasers, semiconductor optical amplifiers, and single-photon emission sources, owing to their discrete atom-like energy states.[1–6] In particular, InAs QD lasers have emerged as promising light sources for the standard O- and C-band optical communications, offering advantages in many key parameters over conventional quantum-well lasers, such as low threshold current densities (J_{th}), temperature insensitivity, low linewidth enhancement factor, and tolerance to crystal defects.[1,3,7–14] Recently, significant advances in high-performance O-band InAs/GaAs QD lasers have been made, even with heteroepitaxial approaches on a silicon-based platform.[15–17]

However, the development of C-band InAs/InP QD lasers, necessary for long-haul communications and eye-safe sensing applications, is still hampered by the severe QD shape inhomogeneity caused by the readily occurring formation of elongated nanostructures in the [1$\bar{1}$0] direction, as well as insufficient gain and high threshold current density for lasers.[18–20] For the InAs/InAlGaAs/InP QD material system commonly used for 1550 nm emission, in particular, the moderate lattice mismatch between InAs and InP (3.2%) and anisotropic surface diffusion of indium adatoms often lead to the formation of quantum dashes rather than round-shaped

QDs, causing the undesired inhomogeneity.[21,22] Although round-shaped QDs can be formed by fine-tuning growth parameters, a severe dispersion in island size persists due to the complex strain distribution.[22,23] This results in a broad full-width at half-maximum (FWHM) of the photoluminescence (PL) spectrum and shifts the peak emission to wavelengths beyond the desired range,[21] thereby posing a challenge in realizing high-performance InAs/InP QD lasers emitting at 1550 nm.

In order to obtain a narrow PL linewidth and near 1550 nm emission, the indium-flush (IF), also known as the double-cap technique, has been previously exploited.[21,24–26] This technique involves separately applying a first capping layer (FCL) and a second capping layer (SCL) after the deposition of QDs, accompanied by an enhanced indium migration or As/P exchange to increase QD uniformity. For example, Luo *et al.*,[25] who optimized the thickness of FCL and the growth temperature of SCL for InAs/InGaAsP/InP QDs grown by metal-organic chemical vapor deposition (MOCVD), reported a reduction in PL linewidth from 124 to 87 meV and a blue shift of peak wavelength from 1690 to 1570 nm. In addition, Shi and Lau[26] demonstrated a narrow room-temperature (RT) PL linewidth of 71 meV for MOCVD-grown InAs/InAlGaAs/InP by optimizing the SCL thickness. However, unlike the O-band InAs/GaAs QD material system,[27–29] the use of the IF method in C-band InAs/InP QDs, particularly with InAlGaAs as the capping layer, has not been well developed, and its comprehensive mechanism remains not fully understood. Moreover, MBE-grown InAs/InAlGaAs/InP QDs employing the IF method, beneficial for achieving high-quality QDs, have been much less explored.

In this work, we studied the impact of the IF technique on the optical and morphological characteristics of MBE-grown InAs/InP QDs with an InAlGaAs quaternary capping layer. The use of the IF technique resulted in the narrowing of RT PL linewidth from 89.2 to 47.9 meV and a blue shift of the peak wavelength from 1824 to 1522 nm, compared with the sample without the IF method. We observed for the first time that, unlike the InAs/GaAs system, Al-rich and In-rich regions were formed during the IF process and then proposed a new evolution model of the IF process on InAs/InAlGaAs/InP QDs. In addition, by exploiting the IF method, broad-area (BA) InAs/InP QD lasers with room-temperature lasing emission around 1600 nm and a low J_{th} per QD layer of 106 A/cm^2 were demonstrated.

II. METHOD

The InAs/InP QD structures were grown using a solid-source Veeco GEN-930 MBE system equipped with a valved arsenic cracker source. The InP (100) substrate wafer was degassed in the buffer chamber at 400 °C for 1 h, followed by a deoxidation step in the growth chamber. The substrate temperature was elevated to 500 °C under As_2 overpressure and held for 1 min to remove surface oxides. Afterward, 400 nm lattice-matched $In_{0.524}Al_{0.476}As$ layers were grown, followed by a 100 nm $In_{0.528}Al_{0.238}Ga_{0.234}As$ layer. The composition of the ternary and quaternary materials was calibrated by x-ray diffraction to ensure the lattice match to InP. Then, the optimized 5.5 monolayers of InAs QDs were deposited at 485 °C.[21] To understand the impact of the IF technique on the optical and structural properties of QDs, sample A without IF and sample B with IF were grown with an otherwise identical growth procedure prior to the capping of QDs. For sample A, a 100 nm InAlGaAs capping layer was subsequently deposited on the QDs at 485 °C as a reference. For sample B, a 4 nm InAlGaAs FCL was deposited with a growth temperature of 485 °C, and subsequently, the substrate temperature was ramped up to 540 °C and held for 1 min. Then, a 96 nm InAlGaAs SCL was grown at 500 °C. The schematic diagram of sample B is illustrated in Fig. 1(a). The PL measurements were taken at RT using a Nanometrics RPM2000 machine with a 635 nm continuous-wave laser at an excitation power density of 430 W/cm^2, and a wavelength-extended InGaAs detector with a cutoff wavelength of 2 μm was used. The surface morphology of the QDs was obtained by atomic force microscopy (AFM). Cross-sectional structural and chemical analysis was carried out by scanning transmission electron microscopy (STEM) and electron energy loss spectroscopy (EELS). Samples were prepared using a conventional focused ion beam, as described for instance in related material systems in Mtunzi *et al.*[30]

The electron microscopy characterization was performed using a probe-corrected Nion UltraSTEM microscope operating at 100 kV. The microscope is equipped with a cold field emission electron source with a nominal energy spread of around 0.3 eV. The electron optics were adjusted to a convergence half-angle of 30 mrad, a beam current of ~40 pA, and a probe size of ~1 Å. High angle annular dark-field (HAADF) (90–190 mrad angular range) images were acquired as a rotational frame series (90° between frames), to eliminate stage drift and scanning distortions using non-rigid registration methods.[31] The EEL spectrum images were acquired with an energy dispersion of 0.725 eV/channel on a Gatan Enfina spectrometer retro-fitted with a Quantum Detectors MerlinEELS hybrid-pixel camera. The dispersion was chosen to allow the acquisition of relevant ionization edges for Al and In, together with the zero-loss peak (ZLP), thus enabling careful energy calibration and multiple-scattering deconvolution for a more precise chemical analysis through EELS. The average spectra from regions of interest were energy-calibrated with respect to the exact position of the ZLP. The spectrum images were subsequently denoised using the principal component analysis routine implemented in the multivariate statistical analysis plugin in Digital Micrograph developed by Watanabe *et al.*[32] Spectral maps were generated by integrating the intensity across suitably large windows above the Al $L_{2,3}$, In $M_{4,5}$, and Ga $L_{2,3}$ EELS edges after the subtraction of the continuously decaying background using a standard power law model. To map the strain field, geometrical phase analysis (GPA) was performed on 2048 × 2048 and 512 × 512 pixel^2 high-resolution HAADF images aligned and averaged from a series of 10 or 20 images to ensure a high signal-to-noise ratio using the commercially available Smart Align[31] and GPA plugin,[33] the latter being based on work by Hÿtch *et al.*,[34] as also detailed in the supplementary material.

III. RESULTS AND DISCUSSION

To characterize the morphology of the uncapped QD surface, AFM was carried out. Figure 1(b) displays a 1 × 1 μm^2 AFM image of sample A, exhibiting a high QD density of 4.9 × 10^{10} cm^{-2} and a dot-like shape with no obvious anisotropic morphologies. The mean height of the QDs observed via AFM is 5.51 nm with an SD of 2.76 nm, showing a relatively large dot size dispersion. To effectively shorten the emission wavelength to the C-band and manipulate the

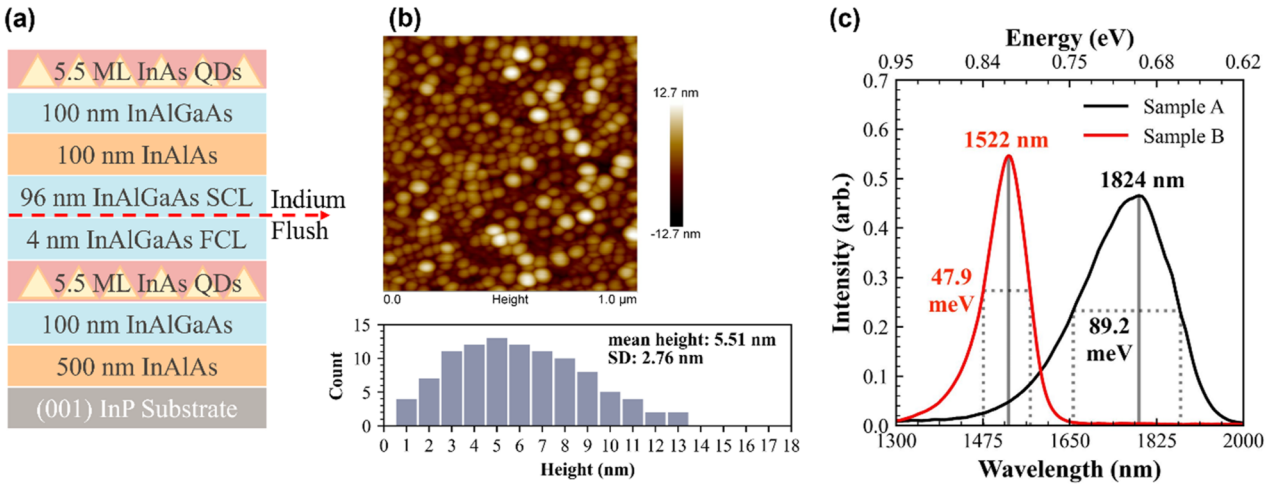

FIG. 1. (a) Schematic diagram of the sample B structure. (b) 1 × 1 μm^2 AFM image of the uncapped QD on the top of sample A, showing a dot density of 4.9 × 10^{10} cm^{-2}. The histogram underneath the AFM image presents the distribution of QD heights. The average height is 5.51 nm, and the standard deviation (SD) is 2.76 nm. (c) RT PL for sample A (black solid line) and sample B (red solid line). The FWHM is indicated by the dashed lines.

dot height uniformity, a 4-nm FCL is chosen, as most QD heights exceed this value. At the same time, the QD height must not be reduced excessively to avoid quenching QD PL emission. Although not shown, a similar QD density is expected for sample B, as it was subjected to identical QD deposition conditions. To investigate the influence of the IF technique on the optical properties of QDs, the RT PL of samples A and B is presented in Fig. 1(c). Without the use of the IF, the peak emission wavelength of sample A is 1824 nm with an FWHM of 89.2 meV, indicating large and inhomogeneous dot sizes. In comparison, the peak emission wavelength of sample B with IF steps blue shifts to 1522 nm, along with a linewidth narrowing from 89.2 to 47.9 meV. It is clear that the employment of the IF process results in the reduction in QD size, facilitating a size quantization-assisted blue shift and simultaneously improving the uniformity of the ensemble.[21,28,35]

To further understand the underlying mechanism for the blue shift in wavelength and the narrowing of the FWHM, HAADF STEM imaging has been employed to examine the in-depth morphology of the QDs with and without the IF process. Figure 2(a) displays a HAADF image of sample A without IF. The previously discussed size dispersion is evident, where the mean QD height is 5.46 nm with a standard deviation (SD) of 0.84 nm. In contrast, the effect of the IF from sample B can be clearly seen in Fig. 2(b). The (001) facets are evident atop the wide QDs, indicating that the IF process introduced a truncation of height from the large QDs exposed by the partial capping (see additional high-resolution HAADF images in Fig. S2). As a result, the mean QD height was decreased to 3.54 nm with an SD of 0.48 nm, contributing to the blue shift and narrow PL linewidth of sample B. Notably, a distinct morphological characteristic was also observed, unlike the models previously reported.[26] That is, the chemically sensitive nature of the HAADF imaging (wherein the contrast scales approximately with atomic number Z as Z^n, n = 1.5–2)[36] suggests that Al-rich (or In-depleted) regions arch between the corners of the truncated QDs, while In-rich regions (brighter-contrast region) form above them. In Fig. 2(c), a high-magnification STEM image of sample B also confirms the presence of lower contrast regions (and thus likely Al-rich) connected to the corners of the truncated QD span above the small, fully encapsulated QD. In addition, an In-rich region in the InAlGaAs SCL matrix is observed above the wide, truncated QD. The chemical nature of these regions as Al-rich and In-rich is confirmed in the EELS maps of three truncated QDs, as shown in Figs. 2(d) and 2(e). An increase in Al-signal (green) connecting the top corners of the truncated QDs is shown in Fig. 2(d), representing the Al-rich (In-depleted) surface of the FCL. A relatively higher concentration of indium (red) is observed directly above all three QDs in Fig. 2(e), but most pronounced in the circled area above the left-most QD, as shown in Fig. 2(e).

Based on our STEM observations, we propose a growth model, displayed in Fig. 3, to elucidate the morphological changes occurring during the overgrowth and the IF step of InAlGaAs-capped InAs QDs. The first step begins with the conventional S–K deposition method of QDs facilitated by a 2D/3D transition upon surpassing a critical thickness; see Fig. 3(a). Figure 3(b) shows the deposition of FCL immediately after the 10 s growth interruption. The QDs whose height is less than 4 nm would be fully encapsulated, while those whose height is larger would be considered "exposed." Consistent with our results and previous work,[27,29,37,38] the elastically relaxed InAs island apices of exposed QDs create energetically unfavorable nucleation sites for Ga and Al adatoms, thereby limiting the FCL growth atop the QDs. Once the surface temperature is increased, the FCL reduces the QD surface energy, forcing a new wetting layer to form on top of the FCL.[29,39] By means of the re-wetting of the exposed QDs, the islands are hence truncated down to the height of the partial cap. The formation of a new wetting layer at IF temperature is illustrated in Fig. 3(c). For the InAlGaAs FCL, the wetting layer is formed by both the re-wetting of the exposed large QDs and desorbed indium segregated from the FCL

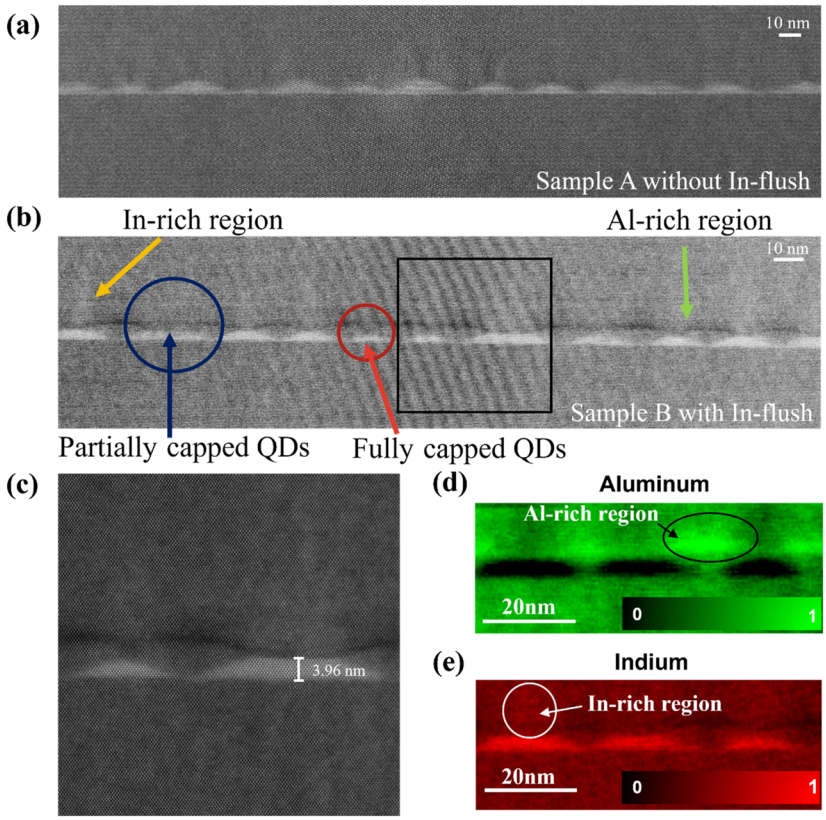

FIG. 2. HAADF images of QD morphologies and adjacent layers of sample A (without IF) in (a) and sample B (with IF) in (b). (c) High-resolution HAADF image of the area highlighted by a black box in *b*, showing fully capped and partially capped QDs. Individual EELS maps of sample B, showing the relative distribution of (d) Al (green intensity channel) and (e) In (red intensity channel).

matrix due to high-temperature annealing.[40] In Fig. 3(d), the partial wetting layer evaporates from the surface,[29] leaving an In-depleted (Al-rich) FCL surface. The InAlGaAs SCL is then deposited atop the truncated QDs and FCL surface, as shown in Figs. 3(e) and 3(f). Indium adatoms incorporate more readily into the SCL matrix immediately above the truncated QDs due to smaller lattice mismatch and thus less compressive strain, as displayed in Fig. 3(e). This proposed mechanism is further supported by strain maps obtained using GPA of the high-resolution HAADF images of both sample types.[34] Figures 4(a) and 4(b) show high-resolution HAADF images

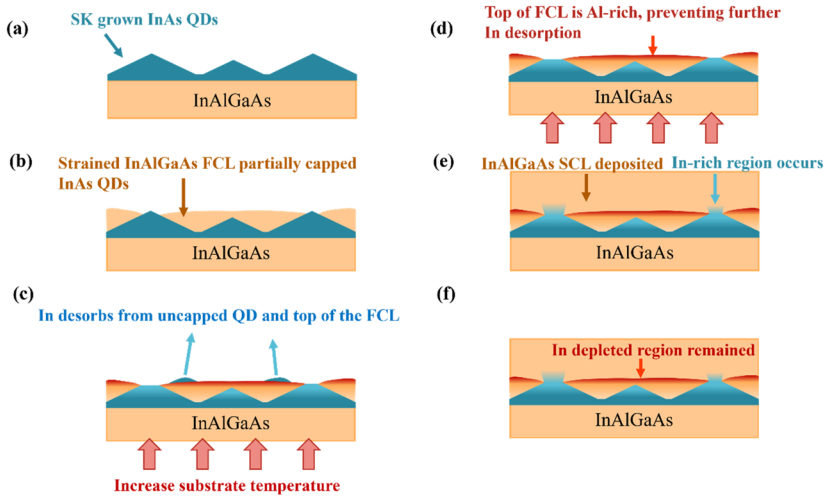

FIG. 3. Schematic illustration of the proposed impact of the IF technique on QDs and adjacent regions. (a) Formation of InAs QDs. (b) The deposition of FCL. (c) The substrate temperature is elevated and indium atoms desorb from both FCL and QDs. (d) Desorbed indium atoms are flushed away. (e) Indium-rich region and (f) indium-depleted (Al-rich) region formed after the deposition of SCL.

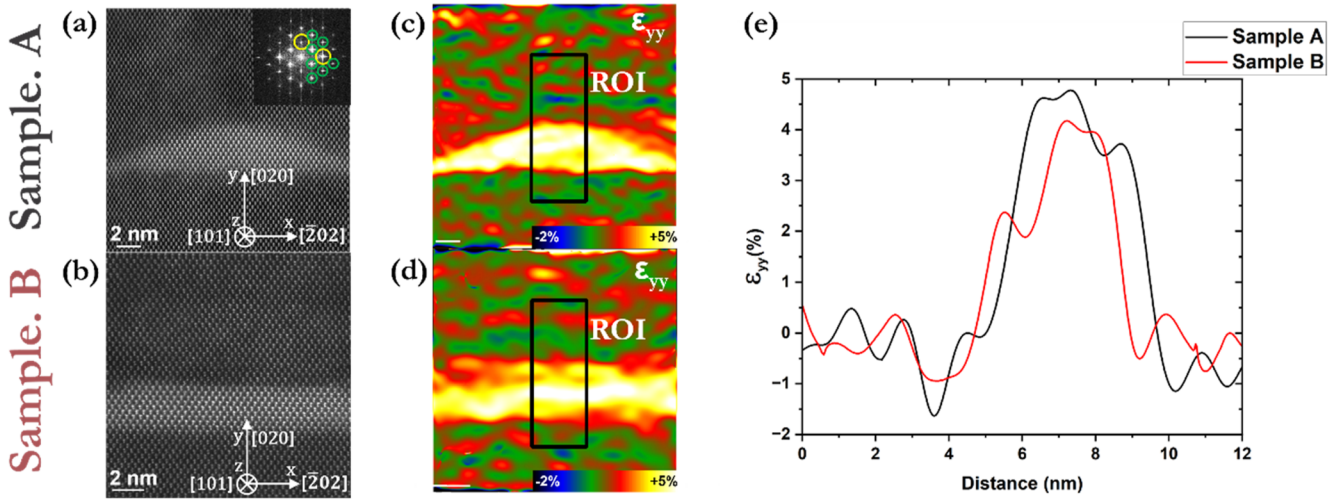

FIG. 4. High-resolution HAADF images of the InAlGaAs/InAs QD/InAlGasAs interface along the [101] axis, as depicted in the FFT inset (a), in (a) sample A (without IF) and (b) sample B (with IF). The vertical ε_{yy} strain maps calculated using GPA from the FFTs of the experimental images in (c) sample A and (d) sample B. (e) The vertical ε_{yy} strain profiles for sample A and sample B along the (200) growth direction of the InAs (QD) on the InAlGaAs matrix averaged along the region of interest highlighted by a rectangle box in (c) and (d), respectively.

of the InAlGaAs/InAs QD/InAlGaAs interface along the [101] axis, with the inset of panel (a) showing the fast Fourier transform (FFT). Figures 4(c) and 4(d) show the vertical ε_{yy} strain maps (along the growth direction) calculated using GPA from the FFTs of the experimental images in panels (a) and (b), respectively. Comparing the averaged vertical ε_{yy} strain profile between sample A (without IF) and sample B (with IF) in Fig. 4(e), a slight reduction in the compressive strain was observed at the interface of sample B with a significant strain relaxation in the InAs QD. Further details are presented in the supplementary material. The In-rich region in the SCL diminishes with deposition thickness, gradually returning toward a nominal equilibrium of the target $In_{0.528}Al_{0.238}Ga_{0.234}As$ composition. Meanwhile, the Al atoms in the SCL segregate to the curved Al-rich surface, promoting the phase separation between In atoms and Al atoms. [41] The low mobility of the Al atoms, caused by the strong reactive property, makes them deposit at the Al-rich region from which they do not migrate further.[42] Finally, Fig. 3(f) illustrates the remaining In-depleted (or Al-rich) region resulting from the indium segregation discussed in Figs. 3(c) and 3(d).

To evaluate the IF technique for InAs/InP QDs in terms of the laser performance, InAs/InP QD laser structures with seven-stack QD layers as an active region were grown based on the optimized InAs/InAlGaAs/InP QD growth with IF. The growth started with the deposition of a 200 nm *n*-type InAlAs:Si, a 200 nm *n*-type InAlGaAs:Si, and a 30 nm undoped InAlGaAs layer, on the *n*-type InP (001) substrate. Subsequently, the seven-stack InAs/InP QD active region was grown with the same parameters used in sample B, except for the 26 nm-thick InAlGaAs SCL. Namely, the InAs QDs and total (4 + 26) nm InAlGaAs capping layers were repeated seven times. Then, a 30 nm undoped InAlGaAs, a 200 nm *p*-type InAlGaAs:Be, a 200 nm p-type InAlAs:Be, a 1700 nm *p*-type InP:Zn cladding, and a 200 nm *p*-type InGaAs:Zn followed. Note that the *p*-InP cladding and *p*-InGaAs contact layers were grown by MOCVD after transferring the wafer from the MBE system. The broad-area (BA) lasers with 50 μm cavity width were fabricated using standard photolithography and the wet etching process. *P*-type Ti/Au (10/250 nm) and *n*-type Ni/AuGe/Ni/Au (10/150/10/250 nm) metal electrodes were deposited on top of the ridge and bottom of the substrate, respectively, and then annealed at 380 °C for 1 min to form an ohmic contact. No wafer thinning or facet coating was applied. The laser bars were cleaved into 500, 750, and 1000 μm cavity lengths.

Figure 5 presents the typical power–current (P–I) curves for the seven-stack InAs/InP QD BA lasers with the IF technique, measured at RT under pulse injection with 1 μs pulse width and 1%

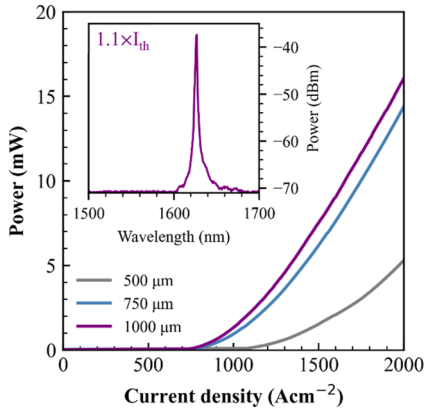

FIG. 5. Single-side pulse P–I plot of seven-stack InAs/InP QD lasers with a cavity width of 50 μm and lengths of 500, 700, and 1000 μm. The inset displays the optical spectrum of 50 × 1000 μm^2 device at an injection current of 1.1 × I_{th}.

duty cycle. The threshold current (I_{th}) and J_{th} for the 500, 750, and 1000 μm devices were measured to be 271 (1085), 292 (777), and 372 mA (742 A/cm^2), respectively, corresponding to the J_{th} per QD layer of 155, 111, and 106 A/cm^2. It is worth mentioning that the J_{th} per QD layer of 106 A/cm^2 achieved here is lower than the value of 126.6 A/cm^2 reported in a recent study on a similar MBE-grown InAs/InAlGaAs/InP QD material system.[43] The inset of Fig. 5 displays the optical spectrum of the 50 × 1000 μm^2 device at an injection current of 1.1 × I_{th}. The lasing peak wavelength is measured to be 1626 nm. Note that the discrepancy between the lasing peak wavelength of the seven-stack InAs/InP QD laser and the PL peak wavelength of the single-layer InAs/InP QDs [Fig. 1(c)] can be attributed to the increase in average size of QDs in the higher-numbered stacking layers due to the enhanced strain coupling.[44,45] This red shift can be reduced with optimized spacer layer thickness, FCL thicknesses, or strain compensation schemes.[46,47]

IV. CONCLUSION

In conclusion, we investigated the effects of the IF technique on the optical and morphological properties of InAs/InP QDs with an InAlGaAs quaternary capping layer, grown by solid-source MBE. It was found that by using IF, the RT PL linewidth narrowed from 89.2 to 47.9 meV and the peak wavelength blue shifted from 1824 to 1522 nm. This is because the large, partially capped QDs are truncated by the IF process, and thus, the reduction in the size of the large QDs leads to a more uniform size distribution. Moreover, it was observed for the first time that Al-rich (In-depleted) and In-rich regions form on the top of the FCL and the truncated QDs, respectively. Following these new observations, we proposed a new model describing the mechanism of the IF process on QDs. In addition, based on the optimized InAs/InAlGaAs/InP QD growth and IF method, the seven-stack InAs/InP QD BA laser structure was grown, and the device with 50 × 1000 μm^2 produced a low J_{th} per QD layer of 106 A/cm^2. These results provide valuable insights into the effective use of the IF method for tailoring the QDs, thus promoting the development of high-performance 1.55 μm InAs/InP QD lasers for the telecom C-band.

SUPPLEMENTARY MATERIAL

Further high-magnification HAADF images and chemical maps of the QDs, along with details on experimental procedures for GPA analysis, are provided in the supplementary material.

ACKNOWLEDGMENTS

The authors acknowledge the support of UK Engineering and Physical Sciences Research Council under Project Nos. EP/X015300/1, EP/W002302/1, EP/V029606/1, EP/V029681/1, EP/T028475/1, EP/S024441/1, EP/Z532848/1, and EP/P006973/1. SuperSTEM is the U.K. National Research Facility for Advanced Electron Microscopy, supported by the Engineering and Physical Sciences Research Council (EPSRC, UK) via Grant Nos. EP/W021080/1 and EP/V036432/1.

AUTHOR DECLARATIONS

Conflict of Interest

The authors have no conflicts to disclose.

Author Contributions

Jiajing Yuan: Conceptualization (equal); Investigation (equal); Methodology (equal); Writing – original draft (equal). **Calum Dear**: Conceptualization (equal); Investigation (equal); Methodology (equal); Writing – original draft (equal). **Hui Jia**: Conceptualization (equal); Investigation (equal); Methodology (equal). **Jae-Seong Park**: Conceptualization (equal); Methodology (equal); Writing – review & editing (equal). **Yaonan Hou**: Methodology (equal). **Khalil El Hajraoui**: Methodology (equal). **Haotian Zeng**: Methodology (equal). **Huiwen Deng**: Methodology (equal). **Junjie Yang**: Investigation (equal); Writing – review & editing (equal). **Mingchu Tang**: Conceptualization (equal); Investigation (equal); Supervision (equal); Writing – review & editing (equal). **Siming Chen**: Investigation (equal); Methodology (equal); Supervision (equal). **Quentin M. Ramasse**: Funding acquisition (lead); Methodology (equal); Resources (equal). **Qiang Li**: Conceptualization (equal); Funding acquisition (lead); Resources (equal); Supervision (equal). **Alwyn Seeds**: Funding acquisition (lead); Supervision (equal). **Huiyun Liu**: Conceptualization (equal); Funding acquisition (lead); Investigation (equal); Resources (equal); Supervision (lead); Writing – review & editing (equal).

DATA AVAILABILITY

The data that support the findings of this study are available from the corresponding authors upon reasonable request.

REFERENCES

[1] M. Asada, Y. Miyamoto, and Y. Suematsu, "Gain and the threshold of three-dimensional quantum-box lasers," IEEE J. Quantum Electron. **22**(9), 1915–1921 (1986).
[2] P. Martyniuk and A. Rogalski, "Quantum-dot infrared photodetectors: Status and outlook," Prog. Quantum Electron. **32**(3–4), 89–120 (2008).
[3] J. Wu, S. Chen, A. Seeds, and H. Liu, "Quantum dot optoelectronic devices: Lasers, photodetectors and solar cells," J. Phys. D: Appl. Phys. **48**(36), 363001 (2015).
[4] V. M. Ustinov, A. E. Zhukov, A. Y. Egorov, and N. A. Maleen, *Quantum Dot Lasers* (Oxford University Press, 2003).
[5] T. Akiyama, M. Sugawara, and Y. Arakawa, "Quantum-dot semiconductor optical amplifiers," Proc. IEEE **95**(9), 1757–1766 (2007).
[6] Y. Arakawa and M. J. Holmes, "Progress in quantum-dot single photon sources for quantum information technologies: A broad spectrum overview," Appl. Phys. Rev. **7**(2), 021309 (2020).
[7] Z. Lv, S. Wang, S. Wang, H. Chai, L. Meng, X. Yang, and T. Yang, "Ultra-high thermal stability InAs/GaAs quantum dot lasers grown on on-axis Si (001) with a record-high continuous-wave operating temperature of 150 °C," Opt. Express **31**(15), 24173–24182 (2023).
[8] A. A. Ukhanov, A. Stintz, P. G. Eliseev, and K. J. Malloy, "Comparison of the carrier induced refractive index, gain, and linewidth enhancement factor in quantum dot and quantum well lasers," Appl. Phys. Lett. **84**(7), 1058–1060 (2004).
[9] Z. Liu, C. Hantschmann, M. Tang, Y. Lu, J.-S. Park, M. Liao, S. Pan, A. Sanchez, R. Beanland, M. Martin, T. Baron, S. Chen, A. Seeds, R. Penty, I. White, and H. Liu,

"Origin of defect tolerance in InAs/GaAs quantum dot lasers grown on silicon," J. Lightwave Technol. **38**(2), 240–248 (2020).
[10]A. Lee, Q. Jiang, M. Tang, A. Seeds, and H. Liu, "Continuous-wave InAs/GaAs quantum-dot laser diodes monolithically grown on Si substrate with low threshold current densities," Opt. Express **20**(20), 22181–22187 (2012).
[11]H. Liu, T. Wang, Q. Jiang, R. Hogg, F. Tutu, F. Pozzi, and A. Seeds, "Long-wavelength InAs/GaAs quantum-dot laser diode monolithically grown on Ge substrate," Nat. Photonics **5**(7), 416–419 (2011).
[12]H. Y. Liu, I. R. Sellers, T. J. Badcock, D. J. Mowbray, M. S. Skolnick, K. M. Groom, M. Gutiérrez, M. Hopkinson, J. S. Ng, J. P. R. David, and R. Beanland, "Improved performance of 1.3 μm multilayer InAs quantum-dot lasers using a high-growth-temperature GaAs spacer layer," Appl. Phys. Lett. **85**(5), 704–706 (2004).
[13]H. Y. Liu, M. Hopkinson, C. N. Harrison, M. J. Steer, R. Frith, I. R. Sellers, D. J. Mowbray, and M. S. Skolnick, "Optimizing the growth of 1.3 μm InAs/InGaAs dots-in-a-well structure," J. Appl. Phys. **93**(5), 2931–2936 (2003).
[14]H. Y. Liu, I. R. Sellers, M. Gutiérrez, K. M. Groom, R. Beanland, W. M. Soong, M. Hopkinson, J. P. R. David, T. J. Badcock, D. J. Mowbray, and M. S. Skolnick, "Optimizing the growth of 1.3-μm InAs/InGaAs dots-in-a-well structure: Achievement of high-performance laser," Mater. Sci. Eng.: C **25**(5–8), 779–783 (2005).
[15]W.-Q. Wei, A. He, B. Yang, Z.-H. Wang, J.-Z. Huang, D. Han, M. Ming, X. Guo, Y. Su, J.-J. Zhang, and T. Wang, "Monolithic integration of embedded III–V lasers on SOI," Light Sci. Appl. **12**(1), 84 (2023).
[16]S. Chen, W. Li, J. Wu, Q. Jiang, M. Tang, S. Shutts, S. N. Elliott, A. Sobiesierski, A. J. Seeds, I. Ross, P. M. Smowton, and H. Liu, "Electrically pumped continuous-wave III–V quantum dot lasers on silicon," Nat. Photonics **10**(5), 307–311 (2016).
[17]J. C. Norman, D. Jung, Z. Zhang, Y. Wan, S. Liu, C. Shang, R. W. Herrick, W. W. Chow, A. C. Gossard, and J. E. Bowers, "A review of high-performance quantum dot lasers on silicon," IEEE J. Quantum Electron. **55**(2), 2000511 (2019).
[18]M. Z. M. Khan, T. K. Ng, and B. S. Ooi, "Self-assembled InAs/InP quantum dots and quantum dashes: Material structures and devices," Prog. Quantum Electron. **38**(6), 237–313 (2014).
[19]V. Sichkovskyi, M. Waniczek, and J. Reithmaier, "High-gain wavelength-stabilized 1.55 μm InAs/InP(100) based lasers with reduced number of quantum dot active layers," Appl. Phys. Lett. **102**(22), 221117 (2013).
[20]P. Caroff, C. Paranthoen, C. Platz, O. Dehaese, H. Folliot, N. Bertru, C. Labbe, R. Piron, E. Homeyer, A. Le Corre, and S. Loualiche, "High-gain and low-threshold InAs quantum-dot lasers on InP," Appl. Phys. Lett. **87**(24), 243107 (2005).
[21]X. Yu, H. Jia, C. Dear, J. Yuan, H. Deng, M. Tang, and H. Liu, "Optically enhanced single- and multi-stacked 1.55 μm InAs/InAlGaAs/InP quantum dots for laser applications," J. Phys. D: Appl. Phys. **56**(28), 285101 (2023).
[22]S. Li, Q. Gong, C. Cao, X. Wang, J. Yan, Y. Wang, and H. Wang, "The developments of InP-based quantum dot lasers," Infrared Phys. Technol. **60**, 216–224 (2013).
[23]A. Ponchet, L. Pedesseau, A. Le Corre, C. Cornet, and N. Bertru, "Shape transition in InAs nanostructures formed by Stranski–Krastanow growth mode on InP (001) substrate," Appl. Phys. Lett. **114**(17), 173102 (2019).
[24]D. Zhou, R. Piron, M. Dontabactouny, O. Dehaese, F. Grillot, T. Batte, K. Tavernier, J. Even, and S. Loualiche, "Low threshold current density of InAs quantum dash laser on InP (100) through optimizing double cap technique," Appl. Phys. Lett. **94**(8), 081107 (2009).
[25]S. Luo, H.-M. Ji, X.-G. Yang, and T. Yang, "Impact of double-cap procedure on the characteristics of InAs/InGaAsP/InP quantum dots grown by metal-organic chemical vapor deposition," J. Cryst. Growth **375**, 100–103 (2013).
[26]B. Shi and K. M. Lau, "Enhanced optical properties of InAs/InAlGaAs/InP quantum dots grown by metal-organic chemical vapor deposition using a double-cap technique," J. Cryst. Growth **433**, 19–23 (2016).
[27]P. Caroff, N. Bertru, C. Platz, O. Dehaese, A. Le Corre, and S. Loualiche, "Emission wavelength control of InAs quantum dots in a GaInAsP matrix grown on InP(311)B substrates," J. Cryst. Growth **273**(3–4), 357–362 (2005).
[28]S. Fafard, Z. Wasilewski, C. N. Allen, D. Picard, M. Spanner, J. McCaffrey, and P. Piva, "Manipulating the energy levels of semiconductor quantum dots," Phys. Rev. B **59**(23), 15368 (1999).
[29]Z. Wasilewski, S. Fafard, and J. McCaffrey, "Size and shape engineering of vertically stacked self-assembled quantum dots," J. Cryst. Growth **201-202**, 1131–1135 (1999).
[30]M. Mtunzi, H. Jia, Y. Hou, X. Yu, H. Zeng, J. Yang, X. Yan, I. Skandalos, H. Deng, J. S. Park *et al.*, "High-quality germanium growth on (111)-faceted V-groove silicon by molecular beam epitaxy," J. Phys. D: Appl. Phys. **57**(25), 255101 (2024).
[31]L. Jones, H. Yang, T. J. Pennycook, M. S. Marshall, S. Van Aert, N. D. Browning, M. R. Castell, and P. D. Nellist, "Smart Align—A new tool for robust non-rigid registration of scanning microscope data," Adv. Struct. Chem. Imaging **1**(1), 8 (2015).
[32]M. Watanabe, E. Okunishi, and K. Ishizuka, "Analysis of spectrum-imaging datasets in atomic-resolution electron microscopy," Microsc. Microanal. **135**, 5 (2009).
[33]HREM Research, Inc., "GPA for DigitalMicrograph—Geometric phase analysis," available at https://www.hremresearch.com/Eng/download/documents/gpa4dm.pdf; accessed on March, 2021.
[34]M. J. Hÿtch, E. Snoeck, and R. Kilaas, "Quantitative measurement of displacement and strain fields from HREM micrographs," Ultramicroscopy **74**(3), 131–146 (1998).
[35]M. Colocci, F. Bogani, L. Carraresi, R. Mattolini, A. Bosacchi, S. Franchi, P. Frigeri, S. Taddei, and M. Rosa-Clot, "Size quantization patterns in self-assembled InAs/GaAs quantum dots," Superlattices Microstruct. **22**(1), 81–84 (1997).
[36]S. J. Pennycook and P. D. Nellist, *Scanning Transmission Electron Microscopy: Imaging and Analysis* (Springer Science & Business Media, 2011).
[37]H. Sasakura, S. Kayamori, S. Adachi, and S. Muto, "Effect of indium-flush method on the control of photoluminescence energy of highly uniform self-assembled InAs quantum dots by slow molecular beam epitaxy growth," J. Appl. Phys. **102**(1), 013515 (2007).
[38]S. Haffouz, S. Raymond, Z. Lu, P. Barrios, D. Roy-Guay, X. Wu, J. Liu, D. Poitras, and Z. Wasilewski, "Growth and fabrication of quantum dots superluminescent diodes using the indium-flush technique: A new approach in controlling the bandwidth," J. Cryst. Growth **311**(7), 1803–1806 (2009).
[39]Q. Xie, P. Chen, and A. Madhukar, "InAs island-induced-strain driven adatom migration during GaAs overlayer growth," Appl. Phys. Lett. **65**(16), 2051–2053 (1994).
[40]K. Radhakrishnan, S. Yoon, R. Gopalakrishnan, and K. Tan, "Indium desorption from strained InGaAs/GaAs quantum wells grown by molecular beam epitaxy," J. Vac. Sci. Technol. A **12**(4), 1124–1128 (1994).
[41]C. Tey *et al.*, "Structural studies of a combined InAlAs–InGaAs capping layer on 1.3-μm Inas/GaAs quantum dots," J. Cryst. Growth **285**(1–2), 17–23 (2005).
[42]P. Ballet, J. Smathers, H. Yang, C. Workman, and G. Salamo, "Control of size and density of InAs/(Al, Ga)As self-organized islands," J. Appl. Phys. **90**(1), 481–487 (2001).
[43]J. Kwoen, N. Morais, W. Zhan, S. Iwamoto, and Y. Arakawa, "All III-arsenide low threshold InAs quantum dot lasers on InP(001)," Electron. Lett. **59**(16), e12920 (2023).
[44]J. S. Kim, "Self-assembled InAs quantum dots with two different matrix materials," J. Cryst. Growth **290**(2), 384–387 (2006).
[45]J. W. Oh, M.-Y. Ryu, B. Jo, J. S. Kim, T. Harris, and Y. K. Yeo, "Bimodal luminescence behavior of spatially-ordered seven-stacked InAs/InAlGaAs quantum dots," Thin Solid Films **541**, 68–71 (2013).
[46]V. Celibert, E. Tranvouez, G. Guillot, C. Bru-Chevallier, L. Grenouillet, P. Duvaut, P. Gilet, P. Ballet, and A. Million, "MBE growth optimization and optical spectroscopy of InAs/GaAs quantum dots emitting at 1.3 μm in single and stacked layers," J. Cryst. Growth **275**(1–2), e2313–e2319 (2005).
[47]K. Akahane, N. Ohtani, Y. Okada, and M. Kawabe, "Fabrication of ultra-high density InAs-stacked quantum dots by strain-controlled growth on InP(311)B substrate," J. Cryst. Growth **245**(1–2), 31–36 (2002).